

Dzyaloshinskii-Moriya anisotropy effect on field-induced magnon condensation in the kagome antiferromagnet α -Cu_{3.26}Mg_{0.74}(OH)₆Br₂

Ying Fu,^{1,2,*} Jian Chen^{3,*}, Jieming Sheng,^{3,*} Han Ge,³ Lianglong Huang,² Cai Liu,² Zhenxing Wang,⁴ Zhongwen Ouyang,⁴ Xiaobin Chen,⁵ Dapeng Yu,² Shanmin Wang,³ Liusuo Wu,³ Hai-Feng Li^{1,†}, Le Wang,^{2,‡} and Jia-Wei Mei^{2,6,§}

¹Institute of Applied Physics and Materials Engineering, University of Macau, Avenida da Universidade Taipa, Macau 999078, China


²Shenzhen Institute for Quantum Science and Engineering, and Department of Physics, Southern University of Science and Technology, Shenzhen 518055, China

³Department of Physics, Southern University of Science and Technology, Shenzhen 518055, China

⁴Wuhan National High Magnetic Field Center and School of Physics, Huazhong University of Science and Technology, Wuhan 430074, China

⁵School of Science and State Key Laboratory on Tunable Laser Technology and Ministry of Industry and Information Technology Key Lab of Micro-Nano Optoelectronic Information System, Harbin Institute of Technology, Shenzhen 518055, China

⁶Shenzhen Key Laboratory of Advanced Quantum Functional Materials and Devices, Southern University of Science and Technology, Shenzhen 518055, China

 (Received 24 August 2021; revised 26 October 2021; accepted 22 November 2021; published 3 December 2021)

We performed a comprehensive electron spin resonance, magnetization, and heat capacity study on the field-induced magnetic phase transitions in the kagome antiferromagnet α -Cu_{3.26}Mg_{0.74}(OH)₆Br₂. With the successful preparation of single crystals, we mapped out the magnetic phase diagrams under the c axis and ab -plane directional magnetic fields B . For $B\parallel c$, three-dimensional (3D) magnon Bose-Einstein condensation (BEC) is evidenced by the power law scaling of the transition temperature, $T_c \propto (B_c - B)^{2/3}$. For $B\parallel ab$, the transition from the canted-antiferromagnetic state to the fully polarized state is a crossover rather than a phase transition, and the characteristic temperature has a significant deviation from 3D BEC scaling. The different behaviors of the field-induced magnetic transitions for $B\parallel c$ and $B\parallel ab$ could result from the Dzyaloshinskii-Moriya (DM) interaction with the DM vector along the c axis, which preserves the c -axis directional spin rotation symmetry and breaks the spin rotation symmetry when $B\parallel ab$. Our findings have the potential to shed light on the investigations of magnetic anisotropy on the field-induced magnon BEC in a quantum antiferromagnet.

DOI: [10.1103/PhysRevB.104.245107](https://doi.org/10.1103/PhysRevB.104.245107)

I. INTRODUCTION

At vanishing chemical potential and temperature, interacting bosons undergo the Bose-Einstein condensation (BEC) transition, which has been realized in ultracold dilute gases [1] and field-induced magnons in quantum antiferromagnets [2–4]. Previous intense investigation of BEC in quantum magnets has been focused on dimerized materials such as TiCuCl₃ [5], BaCuSi₂O₆ [6,7], and Sr₃Cr₂O₈ [8], along with NiCl₂-4SC(NH₂)₂ holding three-dimensional coupled $S = 1$ ion chains [9]. Typically, quantum critical points (QCPs) of transverse magnons that have developed into three-dimensional (3D) BEC show universal evidence $T_c(B) \propto (B_c - B)^{2/3}$ [8–11]. The BEC transition corresponds to the $U(1)$ symmetry spontaneous breaking. In the Bose gas system, the particle conservation guarantees continuous $U(1)$ symmetry whose breaking corresponds to the transition to the BEC state. Without the magnetic anisotropic interactions, a quantum antiferromagnet with magnetic fields above the

saturation field B_c has $U(1)$ spin rotation symmetry along the field direction, and the elementary magnetic excitation, i.e., the magnon, has a gap that is controlled by the field strength. With decreasing magnetic fields, the gap vanishes at the saturation field B_c , and the magnon undergoes the BEC transition with $U(1)$ symmetry breaking. In real materials, spin-orbit coupling gives rise to the magnetic anisotropic term in the quantum magnetism that breaks the $U(1)$ symmetry and modifies the spontaneous transition to a BEC state for the magnon condensation [4]. Since the symmetry-breaking terms are usually small enough, their effect on the magnon condensation near the saturation field is scarcely investigated.

In this paper, we study the magnetic anisotropy effect on field-induced magnon condensations in the kagome antiferromagnet α -Cu_{3.26}Mg_{0.74}(OH)₆Br₂. From a previous study on powder samples [12], α -Cu₃Mg(OH)₆Br₂ has a predominant intralayer ferromagnetic interaction characterized by a Curie-Weiss temperature $\theta = 34$ K and a moderate interlayer antiferromagnetic interaction corresponding to a saturated field of 2 T. The magnetic structure is analogous to the kagome ferromagnet Cu(1,3-benzenedicarboxylate) [Cu(1,3-bdc)] [13], with in-plane ferromagnetically ordered spins, oriented parallel to the b axis, and interplane (c -axis direction) antiferromagnetic order.

*These authors contributed equally to this work.

[†]haifengli@um.edu.mo

[‡]wangl36@sustech.edu.cn

[§]meijw@sustech.edu.cn

As discussed theoretically in Ref. [14], ferromagnetic (FM) spins in a kagome lattice are not frustrated and yield a flat-band magnon, which is a high-energy mode and can be affected by an out-of-plane Dzyaloshinskii-Moriya (DM) interaction. The out-of-plane DM interaction gives rise to topological magnon bands when the magnetization \mathbf{M} is parallel to the DM vector \mathbf{D} , but results in anharmonic particle-nonconserving magnon couplings when $\mathbf{M} \perp \mathbf{D}$, and can also serve as a $U(1)$ symmetry-breaking term for the spin Hamiltonian. Since $U(1)$ spin rotation symmetry is crucial for the magnon BEC, the DM interacting term plays different roles in the magnon condensations near the saturation field for the c -axis directional and in-plane fields. Our main task in this paper is to study the magnetic anisotropy effect on the magnon condensation in α - $\text{Cu}_{3.26}\text{Mg}_{0.74}(\text{OH})_6\text{Br}_2$. The actual chemical formula α - $\text{Cu}_{3.26}\text{Mg}_{0.74}(\text{OH})_6\text{Br}_2$ provides an opportunity to discuss the off-stoichiometric disorder effect on magnon condensations.

The rest of the paper is organized as follows. We present the results in the Sec. II. We summarize our experimental methods for the sample growth and characterization, magnetization and heat capacity measurements, and the electron spin resonance (ESR) in Sec. II A. From a comprehensive understanding of the magnetization and ESR measurements, we write down the spin model as Eq. (1) for α - $\text{Cu}_{3.26}\text{Mg}_{0.74}(\text{OH})_6\text{Br}_2$ in Sec. II B, and the amplitudes of the interactions are justified. In Sec. II C, we map out the magnetic phase diagram for $B \parallel c$ from the magnetization and heat capacity measurements in α - $\text{Cu}_{3.26}\text{Mg}_{0.74}(\text{OH})_6\text{Br}_2$. The 3D magnon BEC transition between the fully polarized state and the canted-antiferromagnetic state has been evidenced by the power law exponent in the transition temperature scaling $T_c \propto (B_c - B)^{2/3}$. We also discuss the magnetic off-stoichiometric disorder effect in the magnon BEC in this section. The field-induced phase diagram for the in-plane magnetic field is presented in Sec. II D. At low temperatures, from the fully polarized state to the canted-antiferromagnetic (canted-AFM) state, it is a crossover rather than a sharp phase transition. The phase boundary of the crossover characteristic temperature near the saturation field has a significant deviation from the 3D BEC scaling. We present our conclusions in Sec. III.

II. RESULTS

A. Experimental methods

Single crystals of α - $\text{Cu}_{3.26}\text{Mg}_{0.74}(\text{OH})_6\text{Br}_2$ were grown by the hydrothermal method. A mixture of 15 mmol CuO , 6 mmol MgBr_2 , and 10.8 mmol NH_4F was sealed in a 25-mL Teflon-lined autoclave with 10 mL water. The autoclave was heated to 270°C and cooled to 140°C at a rate of $0.5^\circ\text{C}/\text{h}$. After being washed with de-ionized water, blue-green and millimeter-scale crystals were obtained as shown in the inset of Fig. 1(c). The crystal structure was determined by a Super-Nova Dual Wavelength diffractometer with monochromated $\text{Cu } K\alpha$ radiation ($\lambda = 1.5418 \text{ \AA}$) at room temperature, and the programs of SHELXT [15] and SHELXL [16] were performed to solve and refine the crystal structure. The ratio of Cu/Mg was determined by inductively coupled plasma atomic emission

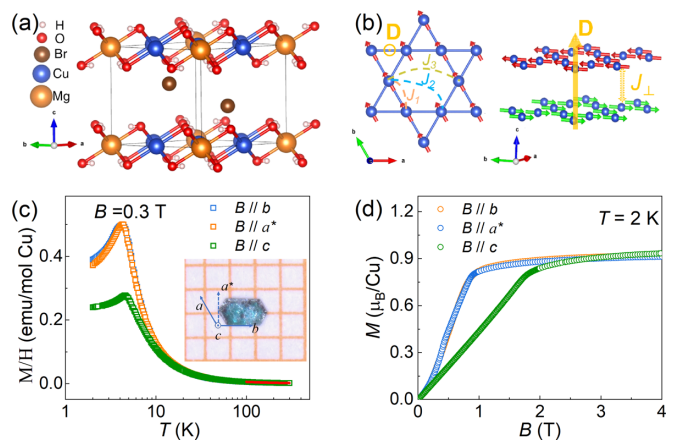


FIG. 1. (a) The crystal structure of α - $\text{Cu}_3\text{Mg}(\text{OH})_6\text{Br}_2$. (b) α - $\text{Cu}_3\text{Mg}(\text{OH})_6\text{Br}_2$ has a predominant intralayer ferromagnetic interaction ($J_1 < 0$) and a moderate interlayer antiferromagnetic interaction ($J_\perp > 0$). The DM interaction has the DM vector ($\mathbf{D} = D_z \hat{z}$) along the c axis (illustrated as a yellow arrow). (c) Temperature-dependent magnetic susceptibilities in α - $\text{Cu}_{3.26}\text{Mg}_{0.74}(\text{OH})_6\text{Br}_2$ for fields along different directions. The red line is the fitting curve to magnetic susceptibilities by the Curie-Weiss law. The inset is a photograph of the single-crystal α - $\text{Cu}_{3.26}\text{Mg}_{0.74}(\text{OH})_6\text{Br}_2$. (d) Field-dependent magnetization at 2 K of α - $\text{Cu}_{3.26}\text{Mg}_{0.74}(\text{OH})_6\text{Br}_2$ with fields along different directions.

spectrometry (ICP-AES) and the chemical composition was confirmed to be α - $\text{Cu}_{3.26}\text{Mg}_{0.74}(\text{OH})_6\text{Br}_2$.

The temperature-dependent magnetization at 0.3 T from 1.8 to 300 K and the field-dependent magnetization with magnetic field increasing and decreasing at 1.8 K were measured by a Quantum Design magnetic property measurement system (MPMS). To study the spin anisotropy, the temperature-dependent magnetization was accomplished along different directions ($B \parallel b$, $B \parallel a^*$, and $B \parallel c$ axes). Massive magnetization curves from 0.4 to 10 K were collected on a Hall sensor magnetometer equipped with a physical property measurement system (PPMS) [17,18]. The temperature- and field-dependent heat capacity measurements were performed on PPMS. The pulsed-field ESR spectra were measured in a field-increasing process along a frequency range of 54–172 GHz at 2 K.

Density functional theory (DFT) [19] has been applied to estimate the exchange parameters in α - $\text{Cu}_3\text{Mg}(\text{OH})_6\text{Br}_2$. First-principles calculations were performed by the Vienna *ab initio* simulation package (VASP) [20–22], choosing the Perdew-Burke-Ernzerhoff revised for solids (PBEsol) functional in a generalized gradient approximation (GGA) [23,24]. A cutoff energy of 620 eV and $6 \times 6 \times 4$ Monkhorst-Pack grids [25] have been used for all calculations. The valence electron pseudopotential of $\text{Cu } 3d$ has been fixed within GGA + U ($U_{3d} = 6 \text{ eV}$) scheme [26]. The lattice constants are fixed and the atomic positions are relaxed, with exchange interactions including the nearest interaction J_1 , the second nearest interaction J_2 , the third nearest interaction J_3 , out-of-plane DM interaction \mathbf{D} , and interlayer AFM interaction J_\perp . J_1 , J_2 , and J_3 are determined from four different ground states, FM, $q = 0$ AFM, cuboc1, and cuboc2 [27] on a $2 \times 2 \times 2$

TABLE I. Crystal data and structure refinement of α -Cu_{3.26}Mg_{0.74}(OH)₆Br₂.

Formula	Cu _{3.26} Mg _{0.74} (OH) ₆ Br ₂
System, space group	Trigonal, $P\bar{3}m1$
Cell parameter	$a = 6.2865 \text{ \AA}$, $c = 6.0795 \text{ \AA}$
Color	Blue-green
Target, wavelength	Mo $K\alpha$, 0.710 73 \AA
Temperature (K)	173
μ (mm ⁻¹)	17.656
$F(000)$	225.8
θ range (deg)	4.97–30.36
$R[F^2 > 2\sigma(F^2)]$,	0.042, 0.096, 1.32
$wR(F^2)$, S	

supercell. For the DM interaction, we compare the energies for negative and positive chiral $q = 0$ AFM configurations. For the interlayer, we double the unit cell along the c axis, and compare the energies for the parallel and antiparallel aligned spins.

B. Exchange interactions and spin anisotropy

As listed in Table I, α -Cu_{3.26}Mg_{0.74}(OH)₆Br₂ crystallizes isostructurally to haydeeite [28], where the Cu ions form a two-dimensional (2D) kagome lattice and the Mg ions settle into the center of the hexagon. According to previous neutron scattering experiments [12], we depict the magnetic structure of α -Cu₃Mg(OH)₆Br₂ as shown in Fig. 1(b).

Figure 1(c) shows the temperature-dependent magnetization with fields of 0.3 T along different crystal directions. From the Curie-Weiss fitting with the g factors extracted from the ESR ($g_{ab} = 1.99$, and $g_c = 2.06$ as shown in Fig. 2), we obtain the Curie-Weiss temperatures $\theta_b = 25.3$ K, $\theta_{a^*} = 27.6$ K, and $\theta_c = 24.4$ K, indicating the predominant

ferromagnetic interactions in α -Cu_{3.26}Mg_{0.74}(OH)₆Br₂. The Curie-Weiss temperatures are smaller than the previously reported values on the powder samples [12], probably due to the off-stoichiometric chemical formula of our samples. There is a clear AFM ordering formed at 4.3 K, implying the AFM interlayer interactions in α -Cu_{3.26}Mg_{0.74}(OH)₆Br₂. We see that the in-plane magnetic susceptibility is larger than the out-of-plane one at low temperatures, implying the easy-plane magnetism in α -Cu_{3.26}Mg_{0.74}(OH)₆Br₂. Figure 1(d) shows the field-dependent magnetization along different crystal directions at $T = 2$ K. The easy-plane and the interlayer AFM interaction can be also derived from the M - B curves for fields along different crystal directions in Fig. 1(d). Despite the zero-field spins orientating towards the b axis, no obvious difference was observed between $B \parallel b$ and $B \parallel a^*$ in both the temperature-dependent and field-dependent magnetization measurements.

Figure 2 presents the ESR spectra collected at 2 K for α -Cu_{3.26}Mg_{0.74}(OH)₆Br₂ with $B \parallel ab$ and $B \parallel c$. The dip in the spectra is the ferromagnetic resonance (FMR) mode. The slopes of the field-frequency relations of the FMR modes are the g factors with values of $g_{ab} = 1.99$ and $g_c = 2.06$. From the magnetization measurement in Fig. 1, we know that the magnetism in α -Cu_{3.26}Mg_{0.74}(OH)₆Br₂ has the easy plane of the kagome plane, accounting for the positive and negative intercepts in the frequency-field-relation lines for the FMR modes with the in-plane and c -axis directional fields, respectively. The easy-plane anisotropic term has the order of 1 K, much smaller than the Curie-Weiss temperature with a value of ~ 25 K.

From the above measurements, we can write down the spin Hamiltonian for α -Cu₃Mg(OH)₆Br₂ as follows,

$$H = J \sum_{n(i,j)} \mathbf{S}_{n,i} \cdot \mathbf{S}_{n,j} + J_{\perp} \sum_{n,i} \mathbf{S}_{n,i} \cdot \mathbf{S}_{n+1,i} + D\hat{z} \cdot \sum_{n(i,j)} (\mathbf{S}_{n,i} \times \mathbf{S}_{n,j}) - g\mu_B B \cdot \sum_{n,i} \mathbf{S}_{n,i}, \quad (1)$$

where $\mathbf{S}_{n,i}$ is the spin operator on the i th site in the n th kagome layers, and (i, j) indicates the nearest-neighbor bonds in the kagome layers. With the help of the DFT calculation on α -Cu₃Mg(OH)₆Br₂, we have obtained the intralayer interactions as $J_1 \simeq -3.5$ meV, $J_2 \simeq -0.18$ meV, and $J_3 \simeq 1.12$ meV. The interlayer AFM interaction J_{\perp} is 0.22 meV and the DM interaction with the vector along the c axis is 1.9 meV. The theoretical values are slightly overestimated, but can be reasonably accepted for a discussion of the magnetic anisotropies. α -Cu_{3.26}Mg_{0.74}(OH)₆Br₂ has the easy-plane anisotropy in the exchange terms, however, in this paper, the DM interaction in α -Cu_{3.26}Mg_{0.74}(OH)₆Br₂ is the main magnetic anisotropy, regarding previous reports on related materials [13,29,30]. The DM interaction has the DM vector $\mathbf{D} = D\hat{z}$ along the c axis and is similar to other kagome magnetic compounds with an energy scale of $D \simeq 10$ K [29,30].

The DM interaction cannot generate fluctuations in the saturated ground state, however, the same is not true for magnon excitations as discussed previously in Ref. [14]. The magnon excitation spectrum is sensitive to the DM interaction and depends on the relative directions of the ground state magnetization and the DM interaction vector.

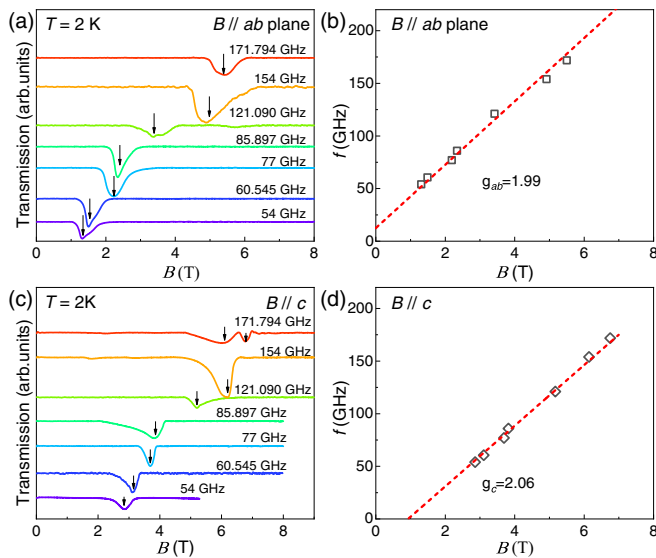


FIG. 2. ESR spectra of α -Cu_{3.26}Mg_{0.74}(OH)₆Br₂ at 2 K for the in-plane field (a) and the c -axis directional field (c). (b) and (d) are the corresponding frequency-field relations obtained from the FMR peaks in the ESR spectra.

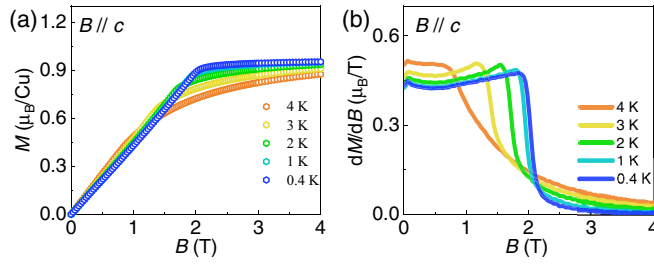


FIG. 3. Field-dependent magnetization M (a) and the corresponding differential susceptibility dM/dB curves (b), at selected temperatures for fields along the c axis.

α -Cu_{3.26}Mg_{0.74}(OH)₆Br₂ has the DM vector along the c axis. For $B \parallel c$ in the fully polarized state, the magnetization is parallel to the DM vector, i.e., $\mathbf{M} \parallel \mathbf{D}$. The DM term provides an imaginary component to the spin-flip hoppings, resulting in the topological magnon bands as observed in neutron scattering studies on Cu[1,3-bdc] [13]. We stress that the DM vector along the c axis preserves the $U(1)$ spin rotation symmetry in the fully polarized state. By contrast, for the in-plane field applied in the fully polarized state, the magnetization is perpendicular to the DM vector, i.e., $\mathbf{M} \perp \mathbf{D}$, and the DM term gives rise to an anharmonic interaction of magnons as it mixes the transverse magnon excitations with the longitudinal ones. The DM interaction here already breaks the $U(1)$ spin rotation symmetry in the fully polarized state.

C. Field-induced magnetic phase diagram for $B \parallel c$

To figure out the field-induced magnetic phases for fields along the c axis, we sweep the magnetic field and measure the magnetization and heat capacity for α -Cu_{3.26}Mg_{0.74}(OH)₆Br₂ as shown in Figs. 3 and 4, respectively, from which the transition from the canted-AFM state to the fully polarized state can be resolved, particularly from the differential results of the magnetization and heat capacity as shown in Fig. 4. Figure 5 summarizes the field-induced phase diagram with the phase boundary between the canted-AFM and the fully polarized states determined from the critical points as shown in Fig. 4. The phase boundary agrees well with the 3D BEC scaling behavior $T_c \propto (B_c - B)^{2/3}$, identifying the 3D BEC quantum criticality of α -Cu_{3.26}Mg_{0.74}(OH)₆Br₂. The 3D magnon BEC condensation behavior is consistent with the theoretical argument in Sec. II B that the DM interaction preserves the $U(1)$

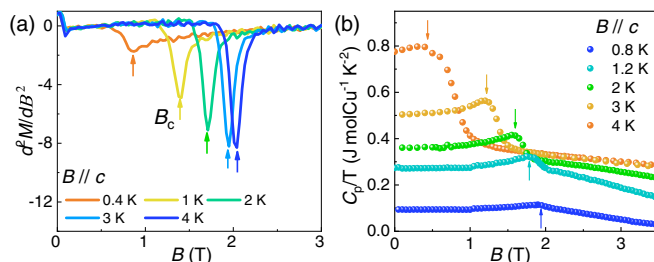


FIG. 4. (a) Second derivative magnetization curves $\frac{d^2M}{dB^2}$ at selected temperatures. (b) Field-dependent specific heat coefficients C_p/T at selected temperatures for fields along the c axis.

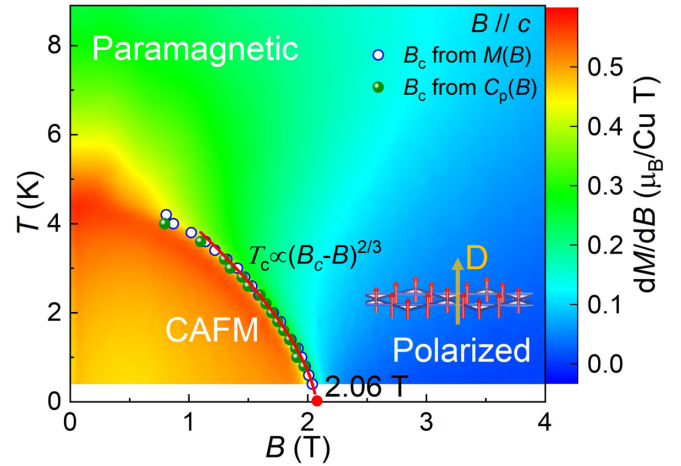


FIG. 5. The magnetic phase diagram for $B \parallel c$. The phase boundaries are determined by critical points B_c from $M(B)$, and $C_p(B)/T$. The red line is a function of $T_c \propto (B_c - B)^{2/3}$, where $B_c = 2.06$ T. The yellow arrow and red arrows are the out-of-plane DM vector and polarized spins. CAFM is an abbreviation of canted-AFM.

spin rotation symmetry along the c axis and the magnon BEC breaks the symmetry spontaneously.

Figure 3(a) shows the field-induced magnetization measurements with fields along the c axis at selected temperatures below the zero-field critical temperature 4.3 K. At the base temperature 0.4 K, the magnetization increases as the field increases and saturates above the saturation field B_c with the fully polarized spins aligned along the c axis. The corresponding differential susceptibility has a small bump at low fields in Fig. 3(b), indicating a crossover from the AFM state to the canted-AFM state. At high magnetic fields, the magnetization saturates and the differential susceptibility exhibits an abrupt jump, implying the transition from the canted-AFM state to the fully polarized state. We swept the fields up and down in the magnetization measurements, and no obvious field-dependent hysteresis behavior was observed. Figure 4(b) is the field-dependent heat capacity and the magnetic phase transition from the canted-AFM state to the fully polarized state was also resolved.

Figure 4(a) shows the second derivative magnetization curves in α -Cu_{3.26}Mg_{0.74}(OH)₆Br₂ for $B \parallel c$. The peak position also determines the saturation field B_c for the magnetic phase transitions from the canted-AFM state to the fully polarized state. Figure 5 shows the field-induced magnetic phase diagram for $B \parallel c$. The intensity of the color code represents the values of the differential magnetic susceptibility $dM/dB(B, T)$, and its boundary coincides with the saturation fields B_c extracted from the peaks as shown in Fig. 4. The phase boundary was well fit by $T_c \propto (B_c - B)^{2/3}$, where $B_c = 2.06$ T, which is hallmark evidence for the 3D BEC of the magnon condensation. It is worth noting that the boundary of $T_c \propto (B_c - B)^{2/3}$ has extended up to 75% of $T_c^{\max} = 4.3$ K, and up to 80% of $T_c^{\max} = 6.25$ K is also reported in the quasi-two-dimensional ferromagnet K₂CuF₄ with critical exponent $\delta = 1$ [31], which is much higher than up to 40% of the maximal ordering temperature in the quantum Monte Carlo (QMC) prediction for spin-dimer systems [32] as well as a

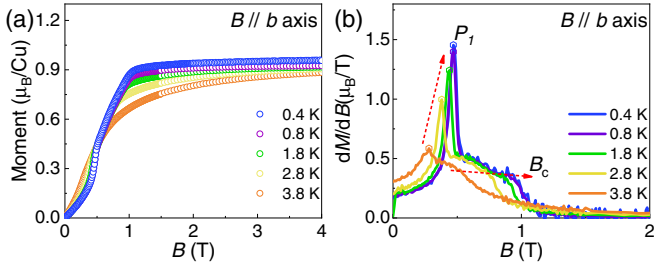


FIG. 6. Field-dependent magnetization M and corresponding differential susceptibility dM/dB curves in (a) and (b), respectively, at selected temperatures for the in-plane fields.

previous experiment on $\text{NiCl}_2\cdot 4\text{SC}(\text{NH}_2)_2$ which shows the critical exponent $2/3$ functions up to 25% of T_c at 1.2 K [33].

For the fully polarized state in $\alpha\text{-Cu}_{3.26}\text{Mg}_{0.74}(\text{OH})_6\text{Br}_2$ with fields along the c axis, the DM interaction in Eq. (1) modifies the spin-flip Hamiltonian as

$$H_{\text{DM}}^{\parallel} = \frac{\tilde{J}}{2} \sum_{n(i,j)} (S_{n,i}^+ S_{n,j}^- e^{i\theta} + S_{n,i}^- S_{n,j}^+ e^{-i\theta}) + \frac{J_{\perp}}{2} \sum_{n,i} (S_{n,i}^+ S_{n+1,i}^- + S_{n,i}^- S_{n+1,i}^+), \quad (2)$$

with $\tilde{J} = -\sqrt{J^2 + D^2}$, and $\theta = \arctan(D/|J|)$. The DM interaction gives an imaginary phase for the spin-flip hopping with the kagome plane and still preserves the $U(1)$ spin rotation symmetry along the c axis. The magnon excitation for the spin-flip Hamiltonian in Eq. (2) gives rise to exotic topological magnon bands [13,14] which deserve future neutron scattering studies of $\alpha\text{-Cu}_{3.26}\text{Mg}_{0.74}(\text{OH})_6\text{Br}_2$. The $U(1)$ spin rotation symmetry breaking results in the 3D magnon BEC transition near the saturation field in $\alpha\text{-Cu}_{3.26}\text{Mg}_{0.74}(\text{OH})_6\text{Br}_2$.

Having established the 3D magnon BEC in $\alpha\text{-Cu}_{3.26}\text{Mg}_{0.74}(\text{OH})_6\text{Br}_2$, we can now use the compound to check the disorder effect in BEC. Since the chemical doping could bring about dirty bosons, the BEC phase boundary may shift and the critical exponent can be further changed [34–36]. The dimensionality of the magnon BEC in $\alpha\text{-Cu}_3\text{Mg}(\text{OH})_6\text{Br}_2$ is $d = 3$. The dynamical exponent for the magnon excitation is $z = 2$ according to Eq. (2), and then the critical scaling exponent for the correlation length $\nu = 1/2$ regarding $\nu z = 1$ due to the symmetry property [37]. Therefore, the BEC quantum criticality here satisfies the Harris criterion $d\nu < 2$, implying the disorder is irrelevant for the quantum phase transition [38]. The actual chemical formula of our sample is $\alpha\text{-Cu}_{3.26}\text{Mg}_{0.74}(\text{OH})_6\text{Br}_2$, but the off-stoichiometric magnetic disorder does not change the critical behavior of the 3D magnon BEC as shown in Fig. 5.

D. Field-induced phase diagram for $B \parallel ab$

To figure out the field-induced magnetic phases for the in-plane fields, we performed magnetization and heat capacity measurements for $\alpha\text{-Cu}_{3.26}\text{Mg}_{0.74}(\text{OH})_6\text{Br}_2$ with fields parallel to the b axis, as shown in Figs. 6 and 7, respectively. Figure 6(a) shows the in-plane field-dependent magnetization

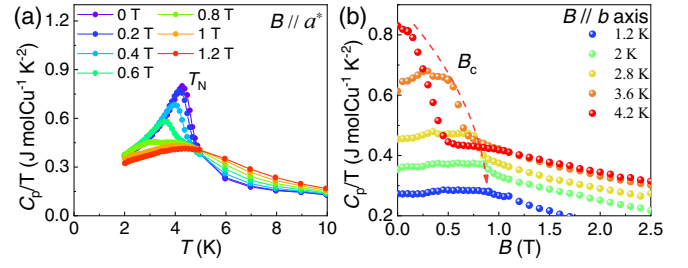


FIG. 7. (a) Temperature-dependent heat capacity for $B \parallel a^*$ with selected fields. (b) Field-dependent specific heat for $B \parallel b$ at selected temperatures.

curves at selected temperatures below T_N of 4.3 K. At $T = 0.4$ K, a steep increase occurs at ~ 0.5 T. By further increasing the fields, the magnetization becomes saturated at $B_c \sim 1$ T. The corresponding differential susceptibility, as shown in Fig. 6(b), has a peak at P_1 and a smooth shoulder at B_c , implying a possible spin-flip transition from the AFM state to the canted-AFM state and a crossover from the canted-AFM state to the fully polarized state, respectively.

Figure 7(a) is the temperature-dependent heat capacity for $B \parallel a^*$ under low fields. A peaklike anomaly at about 4 K is suppressed to low temperatures by the fields, corresponding to the AFM phase transition. The peak is hardly resolved above 0.8 T and evolves into another broad peak that we attribute as a crossover. Figure 7(b) is the field-dependent specific heat for $B \parallel b$ at selected temperatures, in which there is a sudden drop and a smooth crossover at high and low temperatures, respectively.

Figure 8 summarizes the in-plane field-induced magnetic phase diagram of $\alpha\text{-Cu}_{3.26}\text{Mg}_{0.74}(\text{OH})_6\text{Br}_2$. The color intensity represents the value of the differential magnetic susceptibility $dM/dB(B, T)$ as a function of B and T . At high temperatures and low fields, it is a phase transition from the canted-AFM state to the paramagnetic/fully polarized state

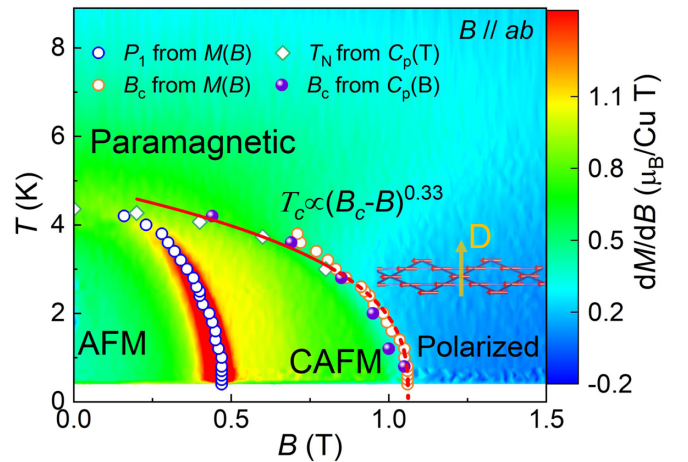


FIG. 8. In-plane field-induced magnetic phase diagram. The red solid and dashed line is fitted by $T_c \propto (B_c - B)^\delta$, with $\delta = 0.33$ and $B_c = 1.06$ T. The yellow arrow and red arrows are the out-of-plane DM vector and polarized spins. Canted-AFM is abbreviated as CAFM.

as represented by the solid line. At low temperatures and high fields, such a transition turns out to be a crossover as represented by the dashed line. The solid and dashed line exhibits a scaling behavior $T_c \propto (B_c - B)^\delta$ with $\delta = 0.33$, $B_c = 1.06$, and a significant deviation from the 3D BEC scaling as shown in Fig. 5. As we mentioned before, chemical doping could modify the critical exponent δ in $T_c \propto (B_c - B)^\delta$, which has been reported in previous studies on $\text{Tl}_{1-x}\text{K}_x\text{CuCl}_3$ [39] and $\text{Ni}(\text{Cl}_{1-x}\text{Br}_x)_2\text{-4SC}(\text{NH}_2)_2$ [36] as well as a recent doping experiment on $\text{BaCuSi}_2\text{O}_6$ [40,41], with δ deviating from $2/3$. However, in $\alpha\text{-Cu}_{3.26}\text{Mg}_{0.74}(\text{OH})_6\text{Br}_2$, the 3D BEC critical exponent $\delta = 2/3$ functions well for $B\parallel c$, as shown in Fig. 5, suggesting the Harris criterion $d\nu < 2$ and possible immunity to chemical disorder for quantum criticality. In fact, it can be ascribed to an out-of-plane DM interaction which has broken the $U(1)$ symmetry of the in-plane Hamiltonian.

For the in-plane fully polarized state in $\alpha\text{-Cu}_{3.26}\text{Mg}_{0.74}(\text{OH})_6\text{Br}_2$, the DM interaction vector is perpendicular to the magnetization and gives rise to the term [14]

$$H_{\text{DM}}^\perp = \frac{D}{2} \sum_{n(i,j)} [(S_{n,i}^+ + S_{n,i}^-)S_{n,j}^z - S_{n,i}^z(S_{n,j}^+ + S_{n,j}^-)], \quad (3)$$

which is a cubic term if we rewrite the spin-flip operator in terms of the Matsubara-Matsuda magnon representation [42]. H_{DM}^\perp is the symmetry-breaking term of uniaxial symmetry and its effect on the magnon spectrum has been carefully studied in Ref. [14]. Such a symmetry-breaking term accounts for the crossover between the canted-AFM state and the fully polarized state in $\alpha\text{-Cu}_3\text{Mg}(\text{OH})_6\text{Br}_2$ for the in-plane fields, and we urge further theoretical investigations on this point.

III. CONCLUSIONS

We have systematically studied the field-induced phase transition in the kagome antiferromagnet $\alpha\text{-Cu}_{3.26}\text{Mg}_{0.74}(\text{OH})_6\text{Br}_2$ and depicted the c -axis and ab -plane magnetic phase diagrams based on the thermodynamic properties. With the $B\parallel c$ axis, a three-dimensional (3D) magnon Bose-Einstein condensation (BEC) occurs at the saturation field B_c between the fully polarized state and the canted antiferromagnetic state and is demonstrated by the power law scaling of the transition temperature, $T_c \propto (B_c - B)^{2/3}$. With the $B\parallel ab$ plane, it is a crossover rather than a phase transition, deviating from 3D BEC scaling. The Dzyaloshinskii-Moriya interaction with the DM vector along the c axis in $\alpha\text{-Cu}_{3.26}\text{Mg}_{0.74}(\text{OH})_6\text{Br}_2$ acts as an “on/off” effect on the particle-conservation term for $M\parallel c$ and $M \perp c$, respectively, and accounts for the different behaviors of the field-induced magnetic phase transitions with the c axis and in-plane fields.

ACKNOWLEDGMENTS

The work at SUSTech was partially supported by the program for Guangdong Introducing Innovative and Entrepreneurial Teams (No. 2017ZT07C062), Shenzhen Key Laboratory of Advanced Quantum Functional Materials and Devices (No. ZDSYS20190902092905285), Guangdong Basic and Applied Basic Research Foundation (No. 2020B1515120100), and China Postdoctoral Science Foundation (No. 2020M682780). Z.W.O. is grateful for the funding of U20A2073. Work at the University of Macau was supported by the Science and Technology Development Fund, Macao SAR (File No. 0051/2019/AFJ), Guangdong Basic and Applied Basic Research Foundation (Guangdong–Dongguan Joint Fund No. 2020B1515120025), and Guangdong–Hong Kong–Macao Joint Laboratory for Neutron Scattering Science and Technology (Grant No. 2019B121205003).

-
- [1] C. J. Pethick and H. Smith, *Bose-Einstein Condensation in Dilute Gases*, 2nd ed. (Cambridge University Press, Cambridge, U.K., 2008).
- [2] E. Batiyev and L. Braginsky, Antiferromagnet in a strong magnetic-field-analogy with a Bose-gas, *JETP* **60**, 781 (1984).
- [3] T. Giamarchi, C. Rüegg, and O. Tchernyshyov, Bose-Einstein condensation in magnetic insulators, *Nat. Phys.* **4**, 198 (2008).
- [4] V. Zapf, M. Jaime, and C. D. Batista, Bose-Einstein condensation in quantum magnets, *Rev. Mod. Phys.* **86**, 563 (2014).
- [5] T. Nikuni, M. Oshikawa, A. Oosawa, and H. Tanaka, Bose-Einstein Condensation of Dilute Magnons in TiCuCl_3 , *Phys. Rev. Lett.* **84**, 5868 (2000).
- [6] S. E. Sebastian, P. A. Sharma, M. Jaime, N. Harrison, V. Correa, L. Balicas, N. Kawashima, C. Batista, and I. R. Fisher, Characteristic Bose-Einstein condensation scaling close to a quantum critical point in $\text{BaCuSi}_2\text{O}_6$, *Phys. Rev. B* **72**, 100404(R) (2005).
- [7] S. Sebastian, N. Harrison, C. Batista, L. Balicas, M. Jaime, P. Sharma, N. Kawashima, and I. Fisher, Dimensional reduction at a quantum critical point, *Nature (London)* **441**, 617 (2006).
- [8] A. A. Aczel, Y. Kohama, C. Marcenat, F. Weickert, M. Jaime, O. E. Ayala-Valenzuela, R. D. McDonald, S. D. Selesnic, H. A. Dabkowska, and G. M. Luke, Field-Induced Bose-Einstein Condensation of Triplons up to 8 K in $\text{InSr}_3\text{Cr}_2\text{O}_8$, *Phys. Rev. Lett.* **103**, 207203 (2009).
- [9] V. S. Zapf, D. Zocco, B. R. Hansen, M. Jaime, N. Harrison, C. D. Batista, M. Kenzelmann, C. Niedermayer, A. Lacerda, and A. Paduan-Filho, Bose-Einstein Condensation of $S = 1$ Nickel Spin Degrees of Freedom in $\text{NiCl}_2\text{-4SC}(\text{NH}_2)_2$, *Phys. Rev. Lett.* **96**, 077204 (2006).
- [10] T. Radu, H. Wilhelm, V. Yushankhai, D. Kovrizhin, R. Coldea, Z. Tylczynski, T. Lühmann, and F. Steglich, Bose-Einstein Condensation of Magnons in Cs_2CuCl_4 , *Phys. Rev. Lett.* **95**, 127202 (2005).
- [11] O. A. Starykh, H. Katsura, and L. Balents, Extreme sensitivity of a frustrated quantum magnet: Cs_2CuCl_4 , *Phys. Rev. B* **82**, 014421 (2010).
- [12] Y. Wei, Z. Feng, C. dela Cruz, W. Yi, Z. Y. Meng, J.-W. Mei, Y. Shi, and S. Li, Antiferromagnetism in the kagome-lattice compound $\alpha\text{-Cu}_3\text{Mg}(\text{OH})_6\text{Br}_2$, *Phys. Rev. B* **100**, 155129 (2019).

- [13] R. Chisnell, J. S. Helton, D. E. Freedman, D. K. Singh, R. I. Bewley, D. G. Nocera, and Y. S. Lee, Topological Magnon Bands in a Kagome Lattice Ferromagnet, *Phys. Rev. Lett.* **115**, 147201 (2015).
- [14] A. L. Chernyshev and P. A. Maksimov, Damped Topological Magnons in the Kagome-Lattice Ferromagnets, *Phys. Rev. Lett.* **117**, 187203 (2016).
- [15] G. M. Sheldrick, SHELXT—integrated space-group and crystal-structure determination, *Acta Crystallogr., Sect. A: Found. Adv.* **71**, 3 (2015).
- [16] G. M. Sheldrick, Crystal structure refinement with SHELXL, *Acta Crystallogr., Sect. C: Struct. Chem.* **71**, 3 (2015).
- [17] A. Cavallini, B. Fraboni, F. Capotondi, L. Sorba, and G. Biasiol, Deep levels in MBE grown AlGaAs/GaAs heterostructures, *Microelectron. Eng.* **73**, 954 (2004).
- [18] A. Candini, G. Gazzadi, A. Di Bona, M. Affronte, D. Ercolani, G. Biasiol, and L. Sorba, Hall nano-probes fabricated by focused ion beam, *Nanotechnology* **17**, 2105 (2006).
- [19] R. O. Jones, Density functional theory: Its origins, rise to prominence, and future, *Rev. Mod. Phys.* **87**, 897 (2015).
- [20] M. Gajdoš, K. Hummer, G. Kresse, J. Furthmüller, and F. Bechstedt, Linear optical properties in the projector-augmented wave methodology, *Phys. Rev. B* **73**, 045112 (2006).
- [21] G. Kresse and J. Furthmüller, Efficient iterative schemes for *ab initio* total-energy calculations using a plane-wave basis set, *Phys. Rev. B* **54**, 11169 (1996).
- [22] J. Hafner, Ab-initio simulations of materials using VASP: Density-functional theory and beyond, *J. Comput. Chem.* **29**, 2044 (2008).
- [23] J. P. Perdew, K. Burke, and M. Ernzerhof, Generalized Gradient Approximation Made Simple, *Phys. Rev. Lett.* **77**, 3865 (1996).
- [24] J. P. Perdew, A. Ruzsinszky, G. I. Csonka, O. A. Vydrov, G. E. Scuseria, L. A. Constantin, X. Zhou, and K. Burke, Restoring The Density-Gradient Expansion For Exchange in Solids and Surfaces, *Phys. Rev. Lett.* **100**, 136406 (2008).
- [25] H. J. Monkhorst and J. D. Pack, Special points for Brillouin-zone integrations, *Phys. Rev. B* **13**, 5188 (1976).
- [26] A. I. Liechtenstein, V. I. Anisimov, and J. Zaanen, Density-functional theory and strong interactions: Orbital ordering in Mott-Hubbard insulators, *Phys. Rev. B* **52**, R5467(R) (1995).
- [27] L. Messio, C. Lhuillier, and G. Misguich, Lattice symmetries and regular magnetic orders in classical frustrated antiferromagnets, *Phys. Rev. B* **83**, 184401 (2011).
- [28] P. Puphal, K. M. Zoch, J. Désor, M. Bolte, and C. Krellner, Kagome quantum spin systems in the atacamite family, *Phys. Rev. Materials* **2**, 063402 (2018).
- [29] A. Zorko, S. Nellutla, J. Van Tol, L. C. Brunel, F. Bert, F. Duc, J.-C. Trombe, M. A. de Vries, A. Harrison, and P. Mendels, Dzyaloshinsky-Moriya Anisotropy in the Spin-1/2 Kagome Compound $\text{ZnCu}_3(\text{OH})_6\text{Cl}_2$, *Phys. Rev. Lett.* **101**, 026405 (2008).
- [30] T. Arh, M. Gomilšek, P. Prelovšek, M. Pregelj, M. Klanjšek, A. Ozarowski, S. J. Clark, T. Lancaster, W. Sun, J.-X. Mi, and A. Zorko, Origin of Magnetic Ordering in a Structurally Perfect Quantum Kagome Antiferromagnet, *Phys. Rev. Lett.* **125**, 027203 (2020).
- [31] S. Hirata, N. Kurita, M. Yamada, and H. Tanaka, Quasi-two-dimensional Bose-Einstein condensation of lattice bosons in the spin- $\frac{1}{2}$ XXZ ferromagnet K_2CuF_4 , *Phys. Rev. B* **95**, 174406 (2017).
- [32] O. Nohadani, S. Wessel, B. Normand, and S. Haas, Universal scaling at field-induced magnetic phase transitions, *Phys. Rev. B* **69**, 220402(R) (2004).
- [33] R. Blinder, M. Dupont, S. Mukhopadhyay, M. S. Grbić, N. Lafforencie, S. Capponi, H. Mayaffre, C. Berthier, A. Paduan-Filho, and M. Horvatić, Nuclear magnetic resonance study of the magnetic-field-induced ordered phase in the $\text{NiCl}_2\text{-}4\text{SC}(\text{NH}_2)$ compound, *Phys. Rev. B* **95**, 020404(R) (2017).
- [34] A. Zheludev and T. Roscilde, Dirty-boson physics with magnetic insulators, *C. R. Phys.* **14**, 740 (2013).
- [35] Z. Yao, K. P. C. da Costa, M. Kiselev, and N. Prokof'ev, Critical Exponents of the Superfluid–Bose-Glass Transition in Three Dimensions, *Phys. Rev. Lett.* **112**, 225301 (2014).
- [36] E. Wulf, D. Hübner, J.-W. Kim, A. Paduan-Filho, E. Ressouche, S. Gvasaliya, V. Zapf, and A. Zheludev, Criticality in a disordered quantum antiferromagnet studied by neutron diffraction, *Phys. Rev. B* **88**, 174418 (2013).
- [37] S. Sachdev, Quantum phase transitions and conserved charges, *Z. Phys. B: Condens. Matter* **94**, 469 (1994).
- [38] A. B. Harris, Effect of random defects on the critical behaviour of Ising models, *J. Phys. C* **7**, 1671 (1974).
- [39] F. Yamada, H. Tanaka, T. Ono, and H. Nojiri, Transition from Bose glass to a condensate of triplons in $\text{Tl}_{1-x}\text{K}_x\text{CuCl}_3$, *Phys. Rev. B* **83**, 020409(R) (2011).
- [40] S. Allenspach, A. Biffin, U. Stuhr, G. S. Tucker, S. Ohira-Kawamura, M. Kofu, D. J. Voneshen, M. Boehm, B. Normand, N. Lafforencie, F. Mila, and C. Ruegg, Multiple Magnetic Bilayers and Unconventional Criticality without Frustration in $\text{BaCuSi}_2\text{O}_6$, *Phys. Rev. Lett.* **124**, 177205 (2020).
- [41] S. Allenspach, P. Puphal, J. Link, I. Heinmaa, E. Pomjakushina, C. Krellner, J. Lass, G. S. Tucker, C. Niedermayer, S. Imajo, Y. Kohama, K. Kindo, S. Kramer, M. Horvatic, M. Jaime, A. Madsen, A. Mira, N. Lafforencie, F. Mila, B. Normand, C. Ruegg, R. Stern, and F. Weickert, Revealing three-dimensional quantum criticality by Sr substitution in Han purple, *Phys. Rev. Research* **3**, 023177 (2021).
- [42] T. Matsubara and H. Matsuda, A lattice model of liquid helium, I, *Prog. Theor. Phys.* **16**, 569 (1956).